JCI The Journal of Clinical Investigation

Essential role of gastric gland mucin in preventing gastric cancer in mice

Fumitoshi Karasawa, … , Kazuhiko Ishihara, Jun Nakayama

J Clin Invest. 2012;122(3):923-934. https://doi.org/10.1172/JCI59087.

Research Article **Oncology**

Gastric gland mucin secreted from the lower portion of the gastric mucosa contains unique*O*-linked oligosaccharides (*O*-glycans) having terminal α1,4-linked *N*-acetylglucosamine residues (αGlcNAc). Previously, we identified human α1,4-*N*-acetylglucosaminyltransferase (α4GnT), which is responsible for the *O*-glycan biosynthesis and characterized αGlcNAc function in suppressing *Helicobacter pylori* in vitro. In the present study, we engineered*A4gnt*$^{-/-}$ mice to better understand its role in vivo. *A4gnt*$^{-/-}$ mice showed complete lack of αGlcNAc expression in gastric gland mucin. Surprisingly, all the mutant mice developed gastric adenocarcinoma through a hyperplasia-dysplasia-carcinoma sequence in the absence of *H. pylori* infection. Microarray and quantitative RT-PCR analysis revealed upregulation of genes encoding inflammatory chemokine ligands, proinflammatory cytokines, and growth factors, such as Ccl2, Il-11, and Hgf in the gastric mucosa of *A4gnt*$^{-/-}$ mice. Further supporting an important role for this *O*-glycan in cancer progression, we also observed significantly reduced αGlcNAc in human gastric adenocarcinoma and adenoma. Our results demonstrate that the absence of αGlcNAc triggers gastric tumorigenesis through inflammation-associated pathways in vivo. Thus, αGlcNAc-terminated gastric mucin plays dual roles in preventing gastric cancer by inhibiting *H. pylori* infection and also suppressing tumor-promoting inflammation.

Essential role of gastric gland mucin in preventing gastric cancer in mice

Fumitoshi Karasawa,[1,2] Akira Shiota,[3] Yukinobu Goso,[4] Motohiro Kobayashi,[1] Yoshiko Sato,[1] Junya Masumoto,[1] Maiko Fujiwara,[1] Shuichi Yokosawa,[5] Takashi Muraki,[5] Shinichi Miyagawa,[2] Masatsugu Ueda,[3] Michiko N. Fukuda,[6] Minoru Fukuda,[6] Kazuhiko Ishihara,[4] and Jun Nakayama[1]

[1]Department of Molecular Pathology, Shinshu University Graduate School of Medicine, Matsumoto, Japan. [2]Department of Surgery, Shinshu University School of Medicine, Matsumoto, Japan. [3]PhoenixBio Co. Ltd., Utsunomiya, Japan. [4]Department of Biochemistry, Kitasato University Graduate School of Medical Sciences, Sagamihara, Japan. [5]Division of Gastroenterology, Iiyama Red Cross Hospital, Iiyama, Japan. [6]Glycobiology Unit, Cancer Research Center, Sanford-Burnham Medical Research Institute, La Jolla, California, USA.

Gastric gland mucin secreted from the lower portion of the gastric mucosa contains unique *O*-linked oligosaccharides (*O*-glycans) having terminal α1,4-linked *N*-acetylglucosamine residues (αGlcNAc). Previously, we identified human α1,4-*N*-acetylglucosaminyltransferase (α4GnT), which is responsible for the *O*-glycan biosynthesis and characterized αGlcNAc function in suppressing *Helicobacter pylori* in vitro. In the present study, we engineered *A4gnt*$^{-/-}$ mice to better understand its role in vivo. *A4gnt*$^{-/-}$ mice showed complete lack of αGlcNAc expression in gastric gland mucin. Surprisingly, all the mutant mice developed gastric adenocarcinoma through a hyperplasia-dysplasia-carcinoma sequence in the absence of *H. pylori* infection. Microarray and quantitative RT-PCR analysis revealed upregulation of genes encoding inflammatory chemokine ligands, proinflammatory cytokines, and growth factors, such as Ccl2, Il-11, and Hgf in the gastric mucosa of *A4gnt*$^{-/-}$ mice. Further supporting an important role for this *O*-glycan in cancer progression, we also observed significantly reduced αGlcNAc in human gastric adenocarcinoma and adenoma. Our results demonstrate that the absence of αGlcNAc triggers gastric tumorigenesis through inflammation-associated pathways in vivo. Thus, αGlcNAc-terminated gastric mucin plays dual roles in preventing gastric cancer by inhibiting *H. pylori* infection and also suppressing tumor-promoting inflammation.

Introduction

Gel-forming mucins covering the gastric mucosa are heavily glycosylated glycoproteins that form a barrier between the stomach and the external environment. Gastric mucins are divided into surface mucin and gland mucin (1). The former is secreted from surface mucous cells lining the gastric mucosa, whereas the latter is produced by gland mucous cells, such as mucous neck cells and pyloric gland cells located in lower layer of the mucosa. Gland mucin characteristically contains *O*-linked oligosaccharides (*O*-glycans) with terminal α1,4-linked *N*-acetylglucosamine residues (αGlcNAc), largely attached to a MUC6 scaffold (2, 3). Interestingly, gland mucin distribution in mammals, including humans, is limited to gland mucous cells of the stomach and Brunner's glands of the duodenum (1, 4).

Previously, we used expression cloning to identify a human A4GNT cDNA encoding α1,4-*N*-acetylglucosaminyltransferase (α4GnT), which is responsible for biosynthesis of these *O*-glycans (5). We also found that α4GnT expression in humans is limited to gastric gland mucous cells and duodenal Brunner's glands, in which αGlcNAc is secreted (3). It is well known that *Helicobacter pylori* is a causative microbe for gastric cancer (6). We then demonstrated in vitro that αGlcNAc suppresses growth and motility of *H. pylori* by inhibiting biosynthesis of the bacterial cell wall constituent, cholesteryl-α-D-glucopyranoside (7). In fact, *H. pylori* rarely colonizes the gastric gland mucin containing αGlcNAc but instead solely colonizes the surface mucin (8). However, the role of αGlcNAc in vivo remained undefined.

Here we generated *A4gnt*$^{-/-}$ mice and found that null mice showed loss of αGlcNAc and developed gastric adenocarcinoma in the absence of *H. pylori* infection. Microarray and quantitative RT-PCR analysis showed upregulation of numerous genes encoding inflammatory chemokine ligands, proinflammatory cytokines, and growth factors in the gastric mucosa of mutant mice. These results demonstrate that αGlcNAc loss in itself is sufficient to trigger gastric tumorigenesis, most likely through inflammation-associated pathways.

Results

A4gnt$^{-/-}$ *mice show complete lack of* αGlcNAc *expression in gastric gland mucin*. To understand the role of αGlcNAc in vivo, we disrupted the *A4gnt* gene encoding α4GnT in mice (Supplemental Figure 1; supplemental material available online with this article; doi:10.1172/JCI59087DS1). After birth, *A4gnt*$^{-/-}$ mice developed to adulthood and reproduced normally. Immunohistochemistry of the gastroduodenal mucosa with a αGlcNAc-specific antibody revealed loss of αGlcNAc in gastric gland mucous cells and in duodenal Brunner's glands in *A4gnt*$^{-/-}$ mice (Figure 1A). Mass spectrometry analysis of *O*-glycans from the gastric mucosa of the glandular stomach demonstrated that the 9 peaks of oligosaccharides carrying αGlcNAc typically detected in wild-type mice were completely absent in *A4gnt*$^{-/-}$ mice (Figure 1B). However, 2 peaks of *O*-glycans, having both sialic acid and fucose residues, appeared, and 2 peaks indicative of oligosaccharides terminated with β-galactose residues were apparently increased in *A4gnt*$^{-/-}$ mice.

A4gnt$^{-/-}$ *mice spontaneously develop gastric adenocarcinoma*. To further analyze the consequences of αGlcNAc loss, we undertook morphological examination of *A4gnt*$^{-/-}$ mice. Surprisingly, histology indicated abnormal proliferation of pyloric epithelial cells in the gastric antrum of mutant mice, even in the absence of oral *H. pylori* administration. In all *A4gnt*$^{-/-}$ mice, tumor growth was noted in the antrum as early as postnatal week 5, and tumor

Conflict of interest: The authors have declared that no conflict of interest exists.
Citation for this article: *J Clin Invest.* 2012;122(3):923–934. doi:10.1172/JCI59087.

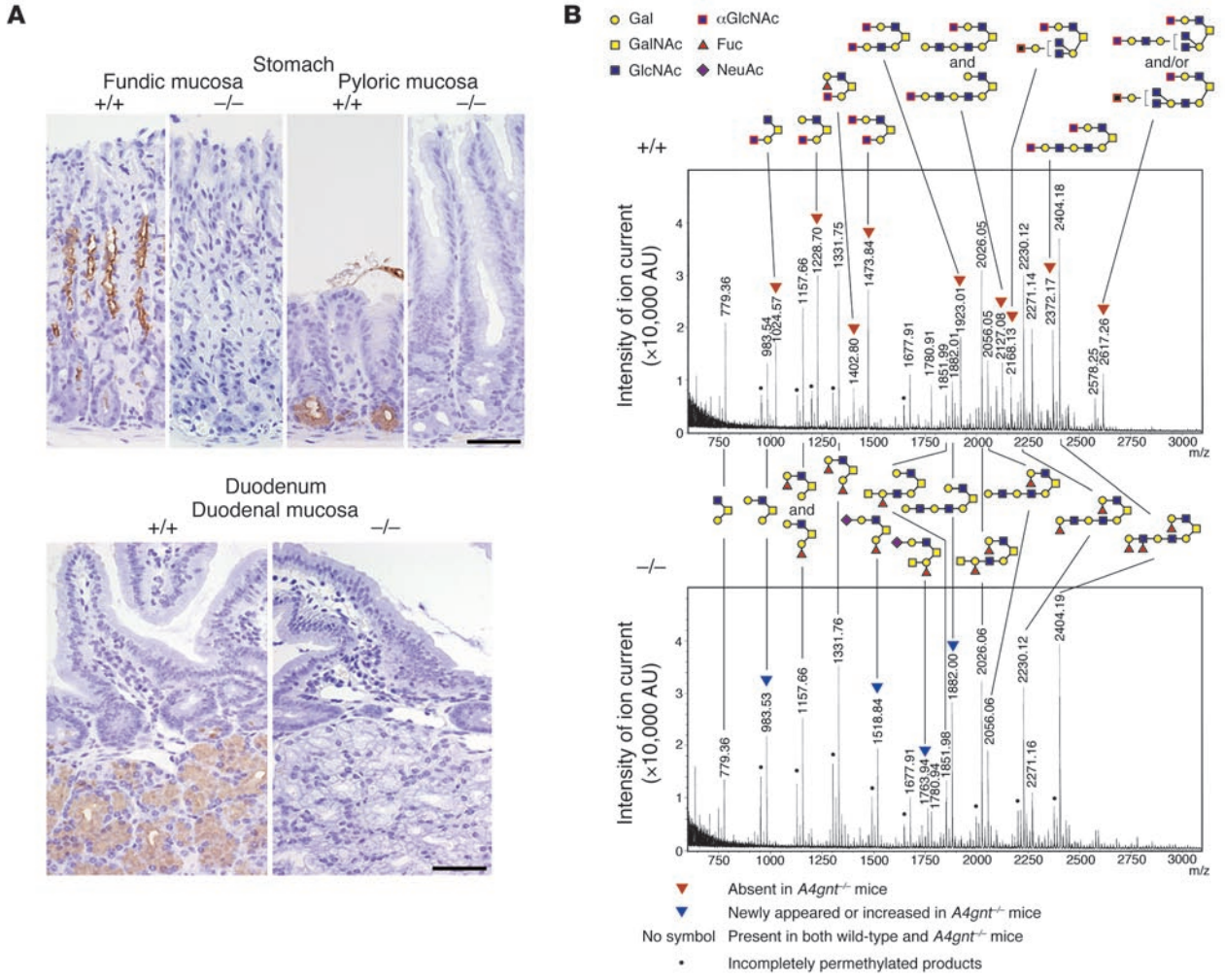

Figure 1

Disappearance of αGlcNAc in *A4gnt*$^{-/-}$ mice. (**A**) Immunohistochemistry with HIK1083 antibody. αGlcNAc is absent in mucous neck cells of the fundic mucosa and pyloric gland cells of the pyloric mucosa in the stomach and Brunner's gland cells of the duodenal mucosa in 10-week-old *A4gnt*$^{-/-}$ mice relative to expression seen in gland mucous cells of age-matched *A4gnt*$^{+/+}$ mice. Scale bar: 50 μm. (**B**) Oligosaccharide analysis of gastric *O*-glycans isolated from 10-week-old *A4gnt*$^{+/+}$ and *A4gnt*$^{-/-}$ mice using MALDI-TOF-MS. Gal, galactose; GalNAc, *N*-acetylgalactosamine; GlcNAc, *N*-acetylglucosamine; Fuc, fucose; NeuAc, *N*-acetylneuraminic acid.

size gradually increased as mice aged (Figure 2, A and B). These tumors were localized to the pyloric mucosa and were never seen in the fundic mucosa of the gastric corpus (Figure 2B and Supplemental Figure 2). Histological examination of the pyloric mucosa revealed that the mucosal thickness of the tumorous portion of *A4gnt*$^{-/-}$ mice was significantly increased compared with that of age-matched wild-type mice ($P < 0.01$) (Figure 2C), and the number of epithelial cells in the tumorous portion was also increased ($P < 0.01$) (Figure 2D). By 5 weeks of age, all *A4gnt*$^{-/-}$ mice developed hyperplasia of both surface mucous cells and pyloric gland cells of the antrum but did not show cellular atypia (Figure 2E and Supplemental Figure 3). By 10 weeks, gastric lesions developed low-grade dysplasia, which showed slight glandular distortion, such as crypt serration or papillary enfolding, with decreased mucin production (Figure 2E). At 20 weeks, gastric pathology proceeded to high-grade dysplasia, characterized by marked glandular complexity, including well-packed tubular gland proliferation with prominent cellular atypia but no intramucosal invasion (Figure 2E). Well-differentiated gastric adenocarcinomas invading the lamina propria developed at 30 weeks in 2 out of 6 *A4gnt*$^{-/-}$ mice, and the incidence of adenocarcinoma increased by 50 weeks of age (Figure 2E and Supplemental Figure 3). All 50-week-old and 60-week-old *A4gnt*$^{-/-}$ mice exhibited adenocarcinoma, with cancer cells mostly located within the gastric mucosa (Figure 2E). Focal submucosal invasion by cancer cells was found in one *A4gnt*$^{-/-}$ mouse at 60 weeks of age (Figure 2B). No distant metastasis was detected in mice observed up to 60 weeks. Undifferentiated types of adenocarcinoma, such as signet ring cell carcinoma, had not developed by 60 weeks of age. Goblet cells expressing MUC2, which are indicative of intestinal metaplasia (9), were rarely detected in the gastric mucosa of the *A4gnt*$^{-/-}$ mice or control *A4gnt*$^{+/+}$ mice during the 60-week observation period (Supplemental Figure 4). No significant abnormality was found in organs other than the glandular stomach (Supplemental Figure 5). These results indicate that loss of αGlcNAc promotes tumor formation of differentiated-type gastric adenocarcinomas, even in the absence of *H. pylori* infection.

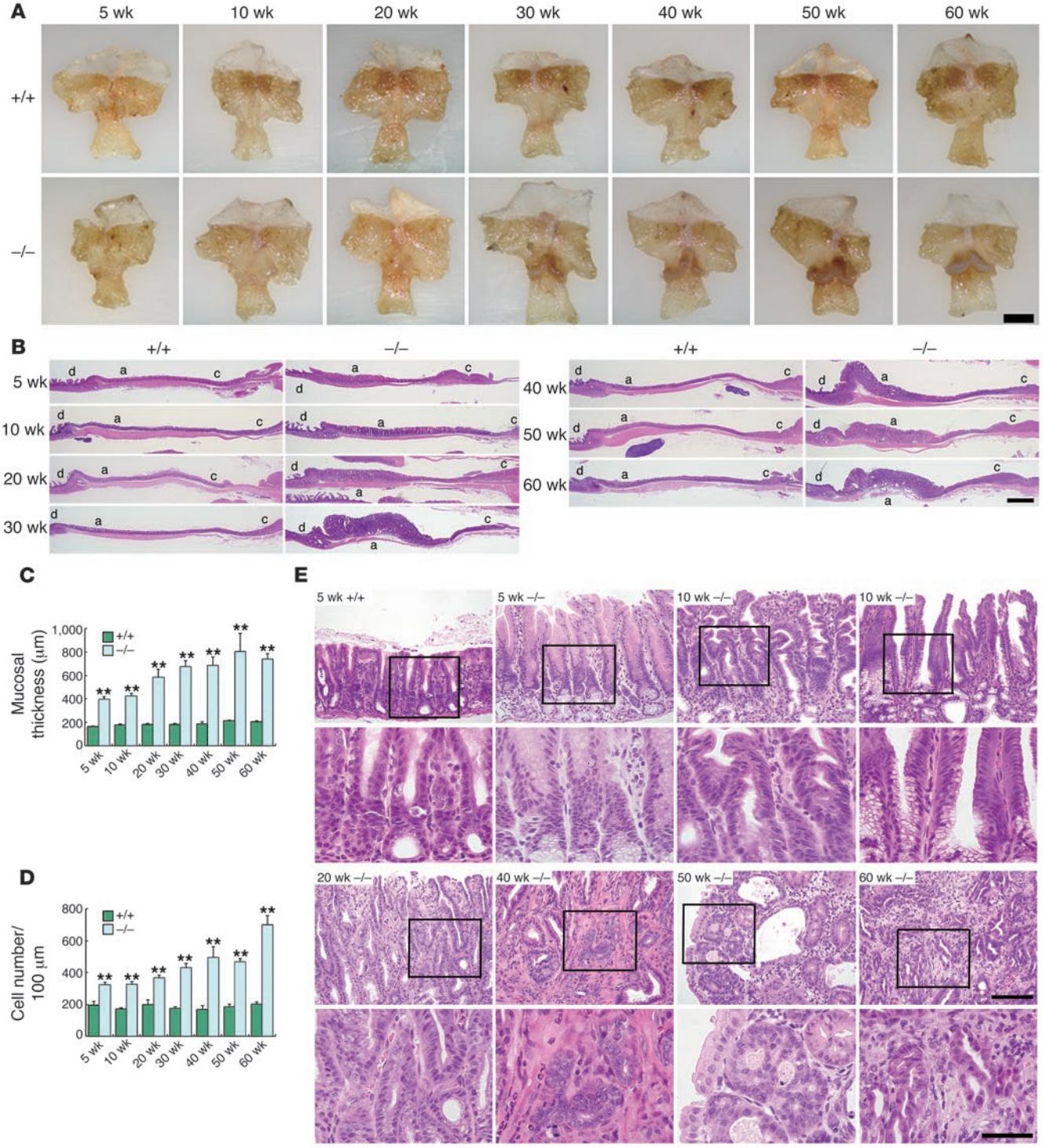

Figure 2

Gastric pathology of *A4gnt*$^{-/-}$ mice. (**A**) Gross appearance of the stomach isolated from *A4gnt*$^{+/+}$ and *A4gnt*$^{-/-}$ mice. Scale bar: 5 mm. (**B**) H&E staining. Low-power view of histology of gastroduodenal mucosa of *A4gnt*$^{+/+}$ and *A4gnt*$^{-/-}$ mice, where c, a, and d indicate the gastric corpus, gastric antrum, and duodenum, respectively. Scale bar: 1 mm. (**C**) Comparison of mucosal thickness of the pyloric mucosa between *A4gnt*$^{+/+}$ and *A4gnt*$^{-/-}$ mice at different ages. Each group consists of 6 mice, and data represent the mean ± SEM. $^{**}P < 0.01$. (**D**) Comparison of epithelial cell number in the pyloric mucosa of *A4gnt*$^{+/+}$ and *A4gnt*$^{-/-}$ mice at different ages. Each group consists of 6 mice, and data represent the mean ± SEM. $^{**}P < 0.01$. (**E**) Histology of hyperplasia (at 5 weeks), low-grade dysplasia (at 10 weeks), high-grade dysplasia (at 20 weeks), and differentiated type of adenocarcinoma (at 40 weeks, 50 weeks, and 60 weeks) seen in the pyloric mucosa of *A4gnt*$^{-/-}$ mice as well as normal pyloric mucosa of 5-week-old *A4gnt*$^{+/+}$ mice. For adenocarcinoma, the desmoplastic reaction in 40-week-old mice, cribriform glands in 50-week-old mice, and irregularly oriented tubular glands in 60-week-old mice are shown. Scale bar: 100 μm. Boxed areas are enlarged in lower panels. Scale bar: 50 μm.

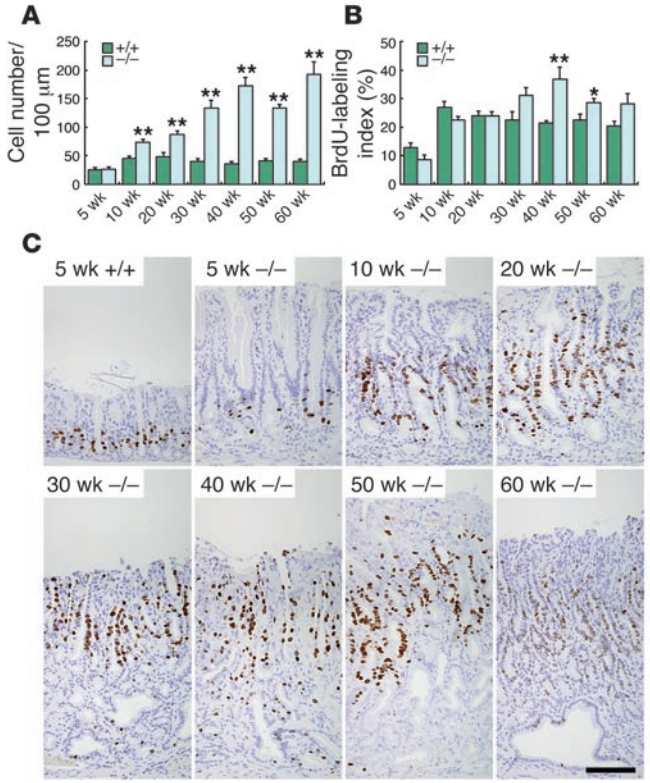

Figure 3
Detection of BrdU-positive S-phase epithelial cells in the pyloric mucosa of *A4gnt*$^{+/+}$ and *A4gnt*$^{-/-}$ mice. (**A**) Comparison of the number of BrdU-positive, S-phase epithelial cells in the pyloric mucosa of *A4gnt*$^{+/+}$ and *A4gnt*$^{-/-}$ mice at different ages. Each group consists of 6 mice, and data represent the mean ± SEM. $^{**}P < 0.01$. (**B**) Comparison of the BrdU-labeling index between *A4gnt*$^{+/+}$ and *A4gnt*$^{-/-}$ mice. Each group consists of 6 mice, and data represent the mean ± SEM. $^{*}P < 0.05$; $^{**}P < 0.01$. (**C**) Localization of S-phase cells in pyloric mucosa. Scale bar: 100 μm.

A4gnt$^{-/-}$ *mice show enhanced proliferation of gastric epithelial cells*. We next compared the proliferative activity of gastric epithelial cells between *A4gnt*$^{-/-}$ and *A4gnt*$^{+/+}$ mice at various ages by injecting BrdU into the abdominal cavity 1 hour prior to sacrifice and undertaking BrdU immunohistochemistry. The number of BrdU-labeled S-phase cells significantly increased in *A4gnt*$^{-/-}$ mice that were older than 6 weeks, compared with that in age-matched wild-type mice ($P < 0.01$) (Figure 3A). The labeling indices of BrdU-labeled cells in *A4gnt*$^{-/-}$ mice were also significantly higher than those in *A4gnt*$^{+/+}$ mice at both 40 and 50 weeks of age ($P < 0.01$ at 40 weeks; $P < 0.05$ at 50 weeks) (Figure 3B), indicating active proliferation of epithelial cells in these periods. In wild-type mice, the distribution of BrdU-labeled S-phase cells was restricted to the generating zone of the pyloric mucosa, whereas, in *A4gnt*$^{-/-}$ mice, they were widely distributed (Figure 3C). In the latter, BrdU-labeled cells were detected primarily in the upper layer of the mucosa; however, a small but substantial number was seen in the glandular base, indicating abnormal distribution of S-phase cells. By contrast, preapoptotic cells, as detected by immunohistochemistry with anti-cleaved caspase-3 antibody, were rarely seen in either *A4gnt*$^{-/-}$ or *A4gnt*$^{+/+}$ mice, and there was no significant difference in their number between the 2 genotypes (Supplemental Figure 6). These results indicate that tumor growth in *A4gnt*$^{-/-}$ mice is largely the result of increased epithelial cell proliferation rather than decreased apoptosis.

Human gastric adenoma and adenocarcinoma show decreased αGlcNAc expression. We next asked whether αGlcNAc expression on its scaffold, MUC6, is reduced in human gastric differentiated-type adenocarcinoma or in the potentially premalignant lesion tubular adenoma. As we demonstrated previously (3) and confirmed here, gland mucous cells expressing MUC6 in non-neoplastic gastric mucosa also expressed αGlcNAc (Figure 4A). Immunohistochemical analysis of gastric adenocarcinoma from 54 patients with differentiated-type early gastric adenocarcinoma (Supplemental Table 1) revealed that MUC6 was expressed in 48 (88.8%) tissue specimens. Among them, 41 (85.4%) patients showed reduced numbers of αGlcNAc-positive cancer cells compared with those of MUC6-positive cancer cells in the same tissue sample (Figure 4, B and C). Notably 19 (39.5%) out of these 48 MUC6-positive patients were completely negative for αGlcNAc (Figure 4D). Semiquantitative analysis showed that the reduction in the number of αGlcNAc-positive cancer cells seen in differentiated types of early gastric cancer is statistically significant compared with the number of MUC6-positive cancer cells ($P < 0.01$) (Figure 4F, left panel). When we used histopathology to classify gastric adenocarcinomas into 2 groups — namely, adenocarcinoma with or without papillary component — significant reductions in αGlcNAc were seen irrespective of the papillary component (Figure 4F, middle and right panels). Subsequently, the same analysis was done on 12 patients with gastric tubular adenoma. Compared with the gastric adenocarcinoma group, both the proportion of MUC6-positive tumors and MUC6 levels were much lower in the gastric adenoma group; specifically, 6 out of 12 (50%) patients were MUC6 positive (Supplemental Table 2). When αGlcNAc expression was compared with that of MUC6 in adenoma cells from MUC6-positive patient specimens ($n = 6$), 5 out of 6 (83.3%) showed no or reduced expression of αGlcNAc (Figure 4E). Semiquantitative analysis showed that αGlcNAc-positive adenoma cells were significantly reduced relative to MUC6-positive adenoma cells ($P < 0.05$) (Figure 4G). Overall, these results suggest that reduced αGlcNAc expression on MUC6 occurs not only in differentiated-type adenocarcinoma but also in tubular adenoma in the human stomach.

The gastric mucosa of A4gnt$^{-/-}$ *mice shows upregulated gene expression of inflammatory chemokine ligands, proinflammatory cytokines, and growth factors*. To elucidate pathways linking αGlcNAc to tumor suppression, DNA microarray analysis was carried out using RNA isolated from gastric mucosa of *A4gnt*$^{-/-}$ and *A4gnt*$^{+/+}$ mice at 5, 10, and 50 weeks of age. Using approximately 2.5×10^4 probes, we identified 209 consistently upregulated genes and 222 consistently downregulated genes in *A4gnt*$^{-/-}$ mice compared with those in *A4gnt*$^{+/+}$ mice during these periods (Supplemental Tables 3 and 4). Gene ontology analysis of these 431 upregulated and downregulated genes identified 22 upregulated genes that encode proteins with receptor binding properties (Table 1). Among them were genes encoding 7 representative molecules, including inflammatory chemokine ligands Cxcl1, Ccl2, and Cxcl5; proinflammatory cytokines Il-1β and Il-11; and growth factors Hgf and Fgf7. Upregulation of all 7 was validated by quantitative RT-PCR analysis of independent samples of glandular stomach mRNA and found to be statistically significant at 10 weeks of age, a time point coinciding with low-grade dysplasia (Figure 5A). Transcript levels encoding the

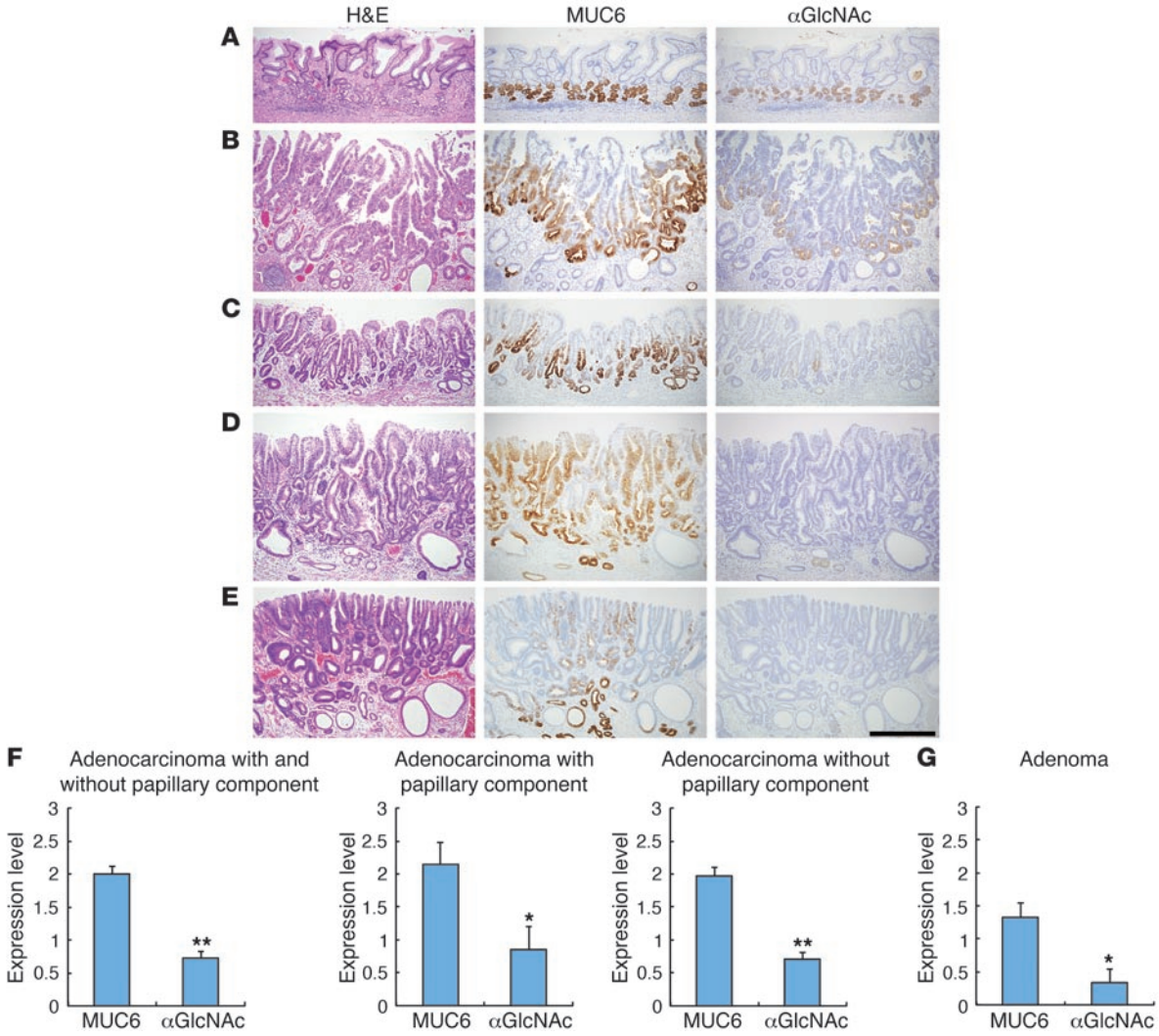

Figure 4
Immunohistochemical expression of MUC6 and αGlcNAc in human pyloric mucosa, gastric differentiated-type adenocarcinoma, and gastric tubular adenoma. (**A**–**E**) Immunohistochemistry with monoclonal antibodies CLH5 for MUC6 and HIK1083 for αGlcNAc. (**A**) MUC6 expression in pyloric glands coincides with that of αGlcNAc in nonneoplastic pyloric mucosa. A normal region of the pyloric mucosa from a patient with undifferentiated-type adenocarcinoma is shown. By contrast, in gastric adenocarcinoma, αGlcNAc expression is reduced compared with that of MUC6. Shown are (**B**) moderate reduction of expression (patient no. 37 in Supplemental Table 1), (**C**) severe reduction of expression (patient no. 30 in Supplemental Table 1), and (**D**) no expression (patient no. 36 in Supplemental Table 1) of αGlcNAc in MUC6-positive adenocarcinoma cells. (**E**) In gastric adenoma, αGlcNAc expression is also reduced compared with that of MUC6: no expression of αGlcNAc is seen in MUC6-positive adenoma cells (patient no. 10 in Supplemental Table 2). Scale bar: 500 μm. Semiquantitation of MUC6 and αGlcNAc expression levels in (**F**) gastric adenocarcinoma and in (**G**) gastric adenoma. $^{*}P < 0.05$; $^{**}P < 0.01$ by Wilcoxon matched-pair test. Data represent the mean ± SEM. Expression level is scored based on the ratio of the number of immunoreactive tumor cells to the total number of tumor cells; 0, no positive cells; 1, less than one-third positive tumor cells; 2, less than two-thirds positive tumor cells; and 3, greater than two-thirds positive tumor cells.

bone morphogenetic protein antagonist gremlin 1 (Grem1) also increased at the 10-week time point, but that upregulation was not statistically significant. Statistically significant upregulation of all 7 genes plus *Grem1* was seen at 50 weeks of age, a time point coinciding with adenocarcinoma. Overall, gene expression changes noted above were not significant at the 5-week time point, except those for *Hgf*, which showed a significant increase in *A4gnt*$^{-/-}$ samples relative to that in controls. The same gene ontology analysis also identified 9 consistently downregulated genes in mutant mice at 5, 10, and 50 weeks of age; these genes encoded proteins with receptor binding properties (Table 2). Significant downregulation of *Amh* and *Egf* in *A4gnt*$^{-/-}$ mice, compared with that in age-matched *A4gnt*$^{+/+}$ mice, was confirmed by quantitative RT-PCR analysis at as early as 5 weeks prior to development of gastric adenocarcinoma (Figure 5B). *Pthlh* was also significantly downregulated in mutant mice relative to that in controls at 10 and 50 weeks.

The gastric mucosa of A4gnt$^{-/-}$ *mice shows increased inflammation and angiogenesis*. The above analysis suggests that tumor-promoting inflammation in the gastric mucosa of *A4gnt*$^{-/-}$ mice underlies tumorigenesis of gastric adenocarcinoma seen in mutant mice. To evaluate the extent of that inflammation, we calculated inflammation scores based on gastric mucosa histology. As expected,

Table 1
Genes upregulated in the gastric mucosa of *A4gnt*$^{-/-}$ mice compared with those in *A4gnt*$^{+/+}$ mice, as revealed by gene ontology analysis

Probe ID	Fold change (5-week-old *A4gnt*$^{-/-}$/ 5-week-old *A4gnt*$^{+/+}$)	Fold change (10-week-old *A4gnt*$^{-/-}$/ 10-week-old *A4gnt*$^{+/+}$)	Fold change (50-week-old *A4gnt*$^{-/-}$/ 50-week-old *A4gnt*$^{+/+}$)	Gene name[A]	Gene symbol
A_52_P481957	29.328596	5.860716	3.7123177	Gremlin 1	*Grem1*
A_51_P363187	26.513502	4.342503	33.988472	Chemokine (C-X-C motif) ligand 1	*Cxcl1*
A_51_P239750	19.9938	13.459662	42.481365	Inhibin β-A	*Inhba*
A_51_P286737	10.460151	3.6093533	8.422346	Chemokine (C-C motif) ligand 2	*Ccl2*
A_51_P267783	9.238376	2.8356814	21.00276	IL-11	*Il11*
A_51_P484998	8.690184	5.990187	4.1379337	HGF	*Hgf*
A_51_P212782	7.9394307	2.135097	16.729721	IL-1β	*Il1b*
A_55_P1985433	7.8159003	4.3436084	5.5367303	Neuregulin 1	*Nrg1*
A_55_P1990032	6.5348234	46.776062	72.16895	Chemokine (C-X-C motif) ligand 5	*Cxcl5*
A_51_P438967	6.5066147	2.0625668	2.7900038	Glycoprotein (transmembrane) nmb	*Gpnmb*
A_52_P355169	5.8783603	2.247188	2.0971909	Tenascin C	*Tnc*
A_51_P436652	5.422487	4.713999	6.310615	Chemokine (C-C motif) ligand 7	*Ccl7*
A_51_P209183	5.3218703	2.1891258	3.0951712	Chemokine (C-X-C motif) ligand 14	*Cxcl14*
A_55_P2035932	4.0948243	7.1590276	2.7109919	FGF7	*Fgf7*
A_52_P460791	4.0006876	13.70317	8.451858	Pancreatic polypeptide	*Ppy*
A_55_P2185905	3.8200583	4.808805	9.85464	Neuregulin 4	*Nrg4*
A_52_P266132	2.8599234	2.8816583	2.2306962	Fibrinogen-like protein 2	*Fgl2*
A_55_P2185900	2.6180248	3.825303	4.3170233	Neuregulin 4	*Nrg4*
A_52_P366462	2.5964735	3.6361988	2.1524127	Peptide YY	*Pyy*
A_55_P2081488	2.454901	6.3133316	3.7940142	Peptidoglycan recognition protein 1	*Pglyrp1*
A_51_P509573	2.371454	2.2198088	2.6153333	Chemokine (C-C motif) ligand 4	*Ccl4*
A_52_P232813	2.1465344	4.85657	5.307726	Chemokine (C-X-C motif) ligand 3	*Cxcl3*

[A]Gene names are listed in descending order based on fold change seen in 5-week-old mice.

infiltration of mononuclear cells was progressively increased as *A4gnt*$^{-/-}$ mice aged and showed significant increases when comparing scores at 5 weeks of age and those at time points later than 10 weeks (Figure 6A). Similarly, neutrophil infiltration was increased but less so than that of mononuclear cells (Figure 6B).

Immunohistochemical analyses revealed that the number of F4/80-positive macrophages in the pyloric mucosa of *A4gnt*$^{-/-}$ mice increased at as early as 5 weeks compared with that in age-matched *A4gnt*$^{+/+}$ mice, and significant numbers of those cells were infiltrated around the atypical glands of 50-week-old *A4gnt*$^{-/-}$ mice ($P < 0.01$) (Figure 6C). The number of CD31-positive endothelial cells in the pyloric mucosa also increased at as early as 5 weeks compared with that in age-matched *A4gnt*$^{+/+}$ mice, and significant numbers of CD31-positive cells were seen in 50-week-old *A4gnt*$^{-/-}$ mice relative to those in wild-type mice ($P < 0.01$) (Figure 6D).

Our microarray data show that *Ptgs2* (encoding prostaglandin-endoperoxide synthase 2, otherwise known as cyclooxygenase-2 [Cox-2]), which plays a key role in inflammation-associated gastric tumorigenesis (10), was substantially upregulated in *A4gnt*$^{-/-}$ mice compared with that in wild-type mice (Supplemental Table 3). To determine whether inflammatory pathways requiring Cox-2 activity promote tumor formation in *A4gnt*$^{-/-}$ mice, we treated 6-week-old *A4gnt*$^{-/-}$ mice for 4 weeks with celecoxib, a selective Cox-2 inhibitor, administered orally. Histological examination revealed that mucosal thickness of the tumorous portion of *A4gnt*$^{-/-}$ mice treated with celecoxib did not differ significantly from that seen in untreated *A4gnt*$^{-/-}$ mice ($P = 0.7775$) (Supplemental Figure 7A). Gastric pathology analysis also revealed that all *A4gnt*$^{-/-}$ mice showed low-grade dysplasia, irrespective of celecoxib treatment (Supplemental Figure 7B). These results suggest that Cox-2 pathways, although upregulated in this mouse model, do not play a significant causative role in tumor-promoting inflammation.

Discussion

To characterize the role of αGlcNAc-terminated mucins in gastric mucosa, we generated *A4gnt*$^{-/-}$ mice. Our studies revealed that α4GnT is the sole enzyme responsible for the biosynthesis of αGlcNAc: both immunohistochemical staining and oligosaccharide analysis (see Figure 1) indicated that αGlcNAc residues are not detected in the gastric mucin secreted from mutant mice. Interestingly, in mutant mice, newly appearing *O*-glycans, exhibiting sialic acid and fucose residues and increased expression of *O*-glycans terminated with β-galactose residues in the gastric mucin, indicate remodeling of *O*-glycans in the gastric mucosa.

More interestingly, abnormal proliferation of gastric pyloric epithelial cells was seen in *A4gnt*$^{-/-}$ mice, and pathology analysis revealed gastric adenocarcinoma through a hyperplasia-dysplasia-carcinoma sequence in the absence of *H. pylori* infection (see Figure 2). Since few gastric cancer models are available, *A4gnt*$^{-/-}$ mice should be useful for in vivo studies of gastric cancer biology. It is also noteworthy that the MUC2-positive goblet cells were rarely seen in the gastric mucosa of either *A4gnt*$^{-/-}$ or control *A4gnt*$^{+/+}$ mice during the 60-week observation period. It remains controversial whether intestinalization of gastric mucosa is preneoplastic or not (11, 12), but the present study clearly indicates that intestinal metaplasia is not associated with gastric tumorigenesis in this model.

The data obtained in the present study clearly indicate that αGlcNAc suppresses gastric tumors in mice, suggesting that αGlcNAc loss has a causative role in gastric cancer. Our findings

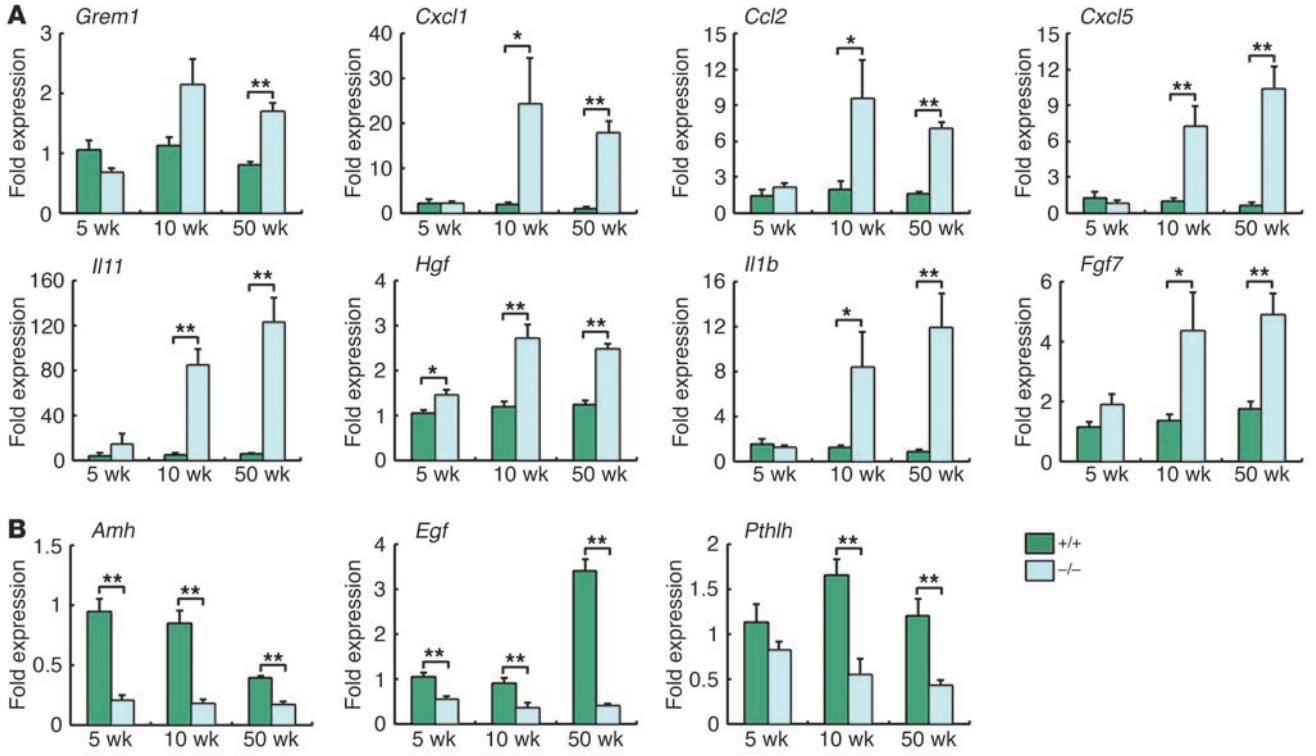

Figure 5
Significantly altered gene expression in *A4gnt*$^{-/-}$ mice compared with that in age-matched *A4gnt*$^{+/+}$ mice, as validated by quantitative RT-PCR analysis. (**A**) Genes upregulated and (**B**) downregulated in independent samples taken from *A4gnt*$^{-/-}$ mice compared with *A4gnt*$^{+/+}$ mice. Fold expression is calculated by setting the median value of expression seen in 5-week-old *A4gnt*$^{+/+}$ mice to 1.0. Data represent the mean ± SEM (n = 5 for 5-week-old *A4gnt*$^{+/+}$ mice; n = 6 for others). *P < 0.05; **P < 0.01.

strongly suggest that this conclusion may also apply to human disease, as expression of αGlcNAc was reduced in human gastric adenocarcinoma and its potentially premalignant lesion adenoma (see Figure 4). Similar results were reported in our previous study, in which 11 patients with the differentiated type of early gastric adenocarcinoma were examined (13). That study also analyzed 9 patients with an undifferentiated type of early gastric cancer and revealed that the number of αGlcNAc-positive adenocarcinoma cells was greater than that of MUC6-positive adenocarcinoma cells. Thus, these findings, combined with results reported here, suggest that αGlcNAc suppresses tumorigenesis of gastric adenoma as well as differentiated-type adenocarcinoma but not undifferentiated gastric adenocarcinoma in humans. Previously, we demonstrated that α4GnT protein is detected in the Golgi apparatus of gastric adenocarcinoma cells expressing αGlcNAc (3, 13). Molecular mechanisms regulating α4GnT expression in gastric cancer cells remain to be determined.

Our DNA microarray analysis identified 209 upregulated genes in *A4gnt*$^{-/-}$ mice compared with those in wild-type mice between 5 and 50 weeks of age. Upregulated genes included 22 that encoded molecules with receptor binding properties (see Table 1). Overall, quantitative RT-PCR analysis demonstrated upregulation of *Grem1*, *Cxcl1*, *Ccl2*, *Cxcl5*, *Il11*, *Hgf*, *Il1b*, and *Fgf7* genes in *A4gnt*$^{-/-}$ mice compared with that in control mice at 10 and 50 weeks of age (see Figure 5A). Among them, the CC chemokine CCL2 (also known as MCP-1) is of particular interest, because CCL2 attracts tumor-associated macrophages (TAMs) (14), which function in protumorigenic immune responses (15, 16). Interestingly, F4/80-positive macrophages were increased in the pyloric mucosa of *A4gnt*$^{-/-}$ mice compared with those in age-matched *A4gnt*$^{+/+}$ mice (see Figure 6C). CCL2 recruitment of TAMs also plays an important role in tumor angiogenesis (14, 17). Genes encoding CXC chemokines CXCL1/CXCL5, which are potent angiogenic factors (14), were also upregulated in *A4gnt*$^{-/-}$ mice (see Figure 5A). In fact, CD31-positive endothelial cells were increased in the pyloric mucosa of *A4gnt*$^{-/-}$ mice compared with those in age-matched *A4gnt*$^{+/+}$ mice (see Figure 6D), indicating that active angiogenesis is occurring in mutant mice. Notably, Ohta et al. (18) demonstrated possible involvement of CCL2 in human gastric adenocarcinoma, showing that CCL2 expression in gastric cancer cells was increased with tumor cell invasiveness, and its expression levels were positively correlated with angiogenesis and macrophage recruitment.

We also observed upregulation of *Il11* in mutant mice (see Figure 5A). Nakayama et al. (19) demonstrated that IL-11 is expressed in 72.6% of human gastric adenocarcinomas from 73 patients and that its expression is significantly higher in differentiated types of adenocarcinoma compared with that in undifferentiated adenocarcinoma. More recently, Howlett et al. (20) demonstrated that IL-11 functions in the progression of inflammation to gastric tumorigenesis via gp130 signaling, followed by STAT3 phosphorylation. The same study revealed that *Grem1* is upregulated in both IL-11–treated mice and human gastric cancer. Here, we found that *Grem1* was significantly upregulated in *A4gnt*$^{-/-}$ mice at 50 weeks of age, a time coinciding with development of adenocarcinoma (see Figure 5A).

Table 2
Genes downregulated in the gastric mucosa of *A4gnt*$^{-/-}$ compared with those in *A4gnt*$^{+/+}$ mice, as revealed by gene ontology analysis

Probe ID	Fold change (5-week-old *A4gnt*$^{-/-}$/ 5-week-old *A4gnt*$^{+/+}$)	Fold change (10-week-old *A4gnt*$^{-/-}$/ 10-week-old *A4gnt*$^{+/+}$)	Fold change (50-week-old *A4gnt*$^{-/-}$/ 50-week-old *A4gnt*$^{+/+}$)	Gene name[A]	Gene symbol
A_55_P2062953	4.890367	4.3170834	2.5092907	Anti-Mullerian hormone	*Amh*
A_52_P38627	4.0518184	4.3469377	6.158944	Epidermal growth factor	*Egf*
A_55_P1974957	2.8989904	5.1364756	6.969068	Tenascin R	*Tnr*
A_51_P129360	2.883138	4.502601	2.493957	Parathyroid hormone-like peptide	*Pthlh*
A_51_P115005	2.868447	3.6097386	2.6505487	Endothelin 1	*Edn1*
A_51_P130475	2.8578	8.47853	5.915544	Wingless-related MMTV integration site 4	*Wnt4*
A_51_P254262	2.5889359	2.4038446	4.1287766	Neurexophilin 3	*Nxph3*
A_55_P1976356	2.3314557	2.1373925	2.0969841	FGF18	*Fgf18*
A_51_P344552	2.0803668	6.2051096	3.5674796	Insulin receptor substrate 4	*Irs4*

[A]Gene names are listed in descending order based on fold change seen in 5-week-old mice.

Recently, Kosinski et al. (21) demonstrated that GREM1 functions to maintain the colonic stem cell niche by activating Wnt signaling and that it is expressed by tumor stromal cells in human colon cancer. Future studies are required to determine the significance of *Grem1* expression in gastric tumorigenesis.

The gene encoding the proinflammatory cytokine IL-1β as well as the genes encoding HFG and FGF7 (also known as keratinocyte growth factor), both of which play important roles in gastric epithelial proliferation (22, 23), were also upregulated in *A4gnt*$^{-/-}$ mice (see Figure 5A). Notably, Palmieri et al. (24) demonstrated that IL-1β induces FGF7 release from breast fibroblasts, and Tu et al. (25) reported that IL-1β overexpressed in mouse gastric mucosa promotes spontaneous gastric inflammation and cancer by recruiting myeloid-derived suppressor cells. In human gastric adenocarcinoma, Kai et al. (26) demonstrated that tumor IL-1β expression levels are elevated more than 50 fold over those seen in normal gastric mucosa and that levels were significantly higher in nonscirrhous carcinomas compared with those in scirrhous carcinomas.

We also identified 9 genes encoding molecules with receptor binding properties that were consistently downregulated at 5, 10, and 50 weeks of age in *A4gnt*$^{-/-}$ mice compared with those in wild-type mice (see Table 2). Overall, quantitative RT-PCR analysis confirmed downregulation of *Amh*, *Egf*, and *Pthlh* genes in mutant mice between 5 and 50 weeks of age (see Figure 5B). Downregulation of *Amh*, which encodes anti-Mullerian hormone (also known as Mullerian-inhibiting substance [MIS]), is noteworthy, because MIS inhibits growth of ovarian and uterine cervical cancer cells (27). The role of MIS in gastric cancer remains unknown and should be addressed in future studies.

Collectively, our results suggest that tumor-promoting inflammation occurs in the gastric mucosa of *A4gnt*$^{-/-}$ mice. The lack of effect of celecoxib treatment on progression of gastric dysplasia in *A4gnt*$^{-/-}$ mice suggests involvement of other signaling pathways promoting inflammation. It remains to be determined how loss of αGlcNAc in gastric gland mucin leads to tumor-promoting inflammation in the stomach.

In conclusion, the present study reveals that αGlcNAc secreted from the gastric gland mucous cells prevents development of differentiated-type gastric adenocarcinoma. *H. pylori* infection is closely associated with gastric cancer in humans (6). We previously demonstrated that gastric gland mucin containing αGlcNAc inhibits *H. pylori* growth and motility, preventing infection of deeper portions of the gastric mucosa (7). The finding that *A4gnt*$^{-/-}$ mice spontaneously develop gastric adenocarcinoma without *H. pylori* infection strongly suggests that αGlcNAc plays dual roles in human gastric cancer development by blocking *H. pylori* infection and suppressing of tumor-promoting inflammation in gastric mucosa. In fact, pyloric gland atrophy, which is associated with reduction of αGlcNAc, reportedly enhances the risk of gastric cancer 2 to 3 fold compared with that of chronic gastritis without pyloric gland atrophy (28). The present study shows an essential role for gastric *O*-glycans that suppress inflammation-associated tumorigenesis, extending our understanding of the function of carbohydrates in pathogenesis (29). These investigations will provide us with new strategies to prevent gastric cancer in humans.

Methods

Patients and clinical gastric samples. The present study included 54 patients with early gastric cancer with differentiated-type adenocarcinomas (33 males and 21 females; age range, 52–90 years) and 12 patients with gastric tubular adenoma (9 males and 3 females; age range, 59–87 years), who underwent endoscopic resection of the primary tumor at Shinshu University Hospital, Matsumoto, Japan, and Iiyama Red Cross Hospital. In all 54 patients, cancer cells were limited to the gastric mucosa. Venous and lymph vessel invasion or lymph node metastasis was absent. Nonneoplastic pyloric mucosa contained in endoscopically resected gastric mucosa from a patient with early gastric cancer with undifferentiated-type adenocarcinoma served as the positive control of immunostaining for αGlcNAc and MUC6. Histopathological diagnosis of gastric tumors was done according to WHO guidelines for classification for gastric carcinoma (30). Formalin-fixed and paraffin-embedded tissue blocks from these patients were retrieved from the archives (between 2007 and 2009) of both hospitals and cut into 3-μm sections.

Generation of A4gnt$^{-/-}$ *mice*. The mouse *A4gnt* BAC clone, RP22-392L18, was selected from an RPCI-22 129S6/SvEv Tac mouse BAC library (BACPAC Resources Center at Children's Hospital Oakland Research Institute) by hybridization of high-density arrayed nylon filters using a 3′ probe generated by PCR with A4GNT3PRF5 and A4GNT3PRR5 primers (Supplemental Table 5). The full-length *A4gnt* genomic sequence was verified by PCR using A4GNT5PRF4 and A4GNT5RRR4 primers for a region 4 kb upstream of exon 1 and A4GNT3PRF5 and A4GNT3PRR5 primers for a region 10 kb downstream of exon 2. The neomycin resistance gene for ES cell selection was introduced into exons 2 and 3 of the BAC clone using a Red/ET Quick & Easy BAC Modification Kit (Gene Bridges). A neomycin-resistance selection cassette (PGK-gb2-neo) flanked on both

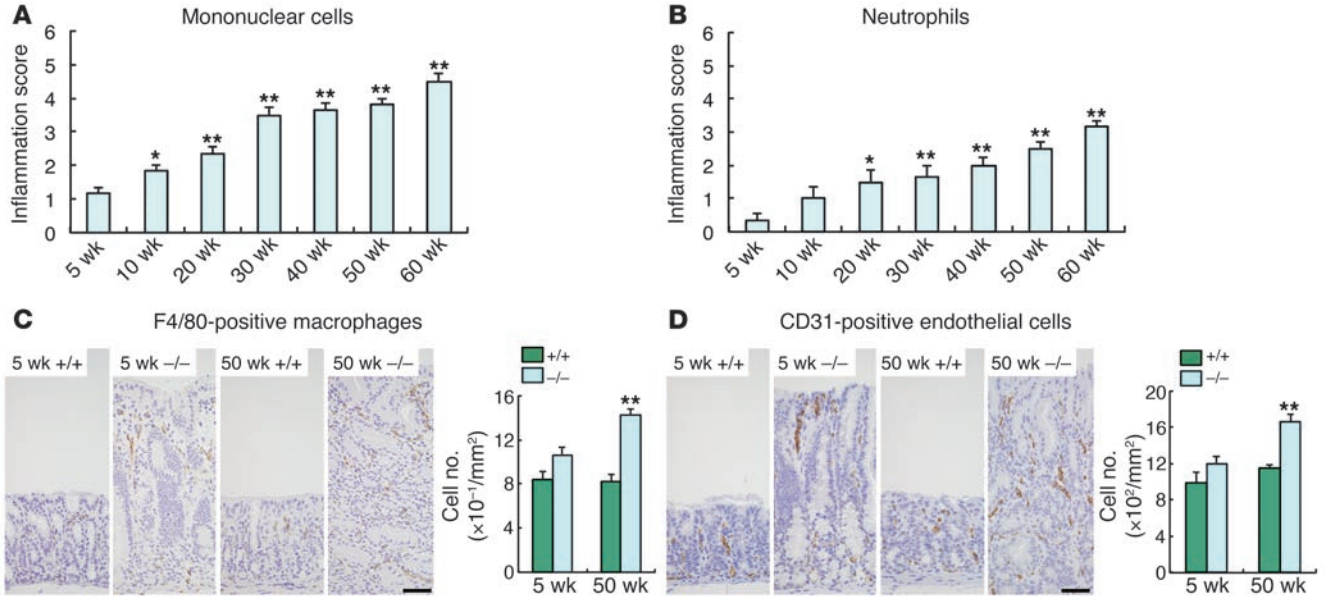

Figure 6

Inflammation and angiogenesis in the gastric mucosa of *A4gnt*$^{-/-}$ mice. (**A**) Inflammation score for mononuclear cell infiltration in the antrum of *A4gnt*$^{-/-}$ mice. Each group consists of 6 mice, and data represent the mean ± SEM. $^{*}P < 0.05$; $^{**}P < 0.01$. (**B**) Inflammation score for neutrophil infiltration in the antrum of *A4gnt*$^{-/-}$ mice. Each group consists of 6 mice, and data represent the mean ± SEM. $^{*}P < 0.05$; $^{**}P < 0.01$. (**C**) Detection of F4/80-positive macrophages in gastric mucosa. Immunohistochemistry with anti-F4/80 antibody (left panel). Scale bar: 50 μm. Comparison of number of F4/80-positive macrophages in gastric mucosa of *A4gnt*$^{+/+}$ and *A4gnt*$^{-/-}$ mice (right panel). Each group consists of 6 mice, and data represent the mean ± SEM. $^{**}P < 0.01$. (**D**) Detection of CD31-positive endothelial cells in gastric mucosa. Immunohistochemistry with anti-CD31 antibody (left panel). Scale bar: 50 μm. Comparison of number of CD31-positive endothelial cells in gastric mucosa of *A4gnt*$^{+/+}$ and *A4gnt*$^{-/-}$ mice (right panel). Each group consists of 6 mice, and data represent the mean ± SEM. $^{**}P < 0.01$.

sides by 50 nucleotides homologous to arm sequences was amplified by PCR using A4GNTBIF1 and A4GNTBIR1 primers. The *A4gnt* targeting vector was constructed in pBluescript-MCA/DTA using a Red/ET BAC Subcloning Kit (Gene Bridges) as described previously (31). The 5′- and 3′-recombination sites of the modified BAC clone were located in a region 4.4 kb upstream and 9.6 kb downstream of the PGK-gb2-neo cassette, respectively. Tandem 5′- and 3′-recombination sequences were made by annealing A4GNTCOF1 and A4GNTCOR1 oligonucleotides and then subcloned into *Spe*I/*Xho*I-cut pBluescript-MCA/DTA plasmid. The resultant tandem 5′- and 3′-recombination sequence was cleaved by *Pme*I to create both homology arms for Red/ET BAC subcloning, and then the *A4gnt* targeting plasmid was sequenced to confirm PGK-gb2-neo cassette insertion (Supplemental Figure 1).

Mouse ES cells (PhoenixBio Co. Ltd.) derived from the 129S6/SvEvTac mouse were cultured with mouse embryo fibroblasts as feeders in medium supplemented with recombinant leukemia inhibitory factor. ES cells were electroporated with the targeting vector, and G418-resistant clones were isolated. To verify homologous recombination at the *A4gnt* locus, genomic DNA isolated from G418-resistant clones was digested with *Bgl*II, *Bst*1107I, and *Eco*RI and subjected to Southern blot analysis with a 5′-probe, 3′-probe, and neo-probe, respectively. The 5′-probe was generated by PCR with A4GNT5PRF4 and A4GNT5PRR4 primers, and the neo-probe was prepared by excising the neomycin-resistance gene from pKO-NTKV-1901 (Stratagene) with *Pvu*II and *Xba*I. All probes used for Southern blotting were prepared by random-prime labeling using the Megaprime DNA Labeling System (GE Healthcare). C57BL/6J blastocysts injected with correctly targeted ES cells were implanted into pseudopregnant CD-1 females to produce mutant mice. Chimeric male offspring were identified on the basis of coat color and bred with C57BL/6J female mice. Germ line transmission of the mutant *A4gnt* locus was assessed by Southern blotting of *Bgl*II-digested tail DNA as described above. Heterozygotes were crossed to generate homozygous mutants. *A4gnt*$^{-/-}$ mice backcrossed into a C57BL/6J background for 6 generations (F6 mice) were used in this study. Southern blot analysis of genomic DNA isolated from the tails of F6 mice confirmed correct targeting of the *A4gnt* gene (Supplemental Figure 1). F6 mutant mice were genotyped by multiplex PCR using tail DNA and a set of 3 primers for the short arm (SAC-F and SAN-R or SAW-R), yielding 559-bp and 253-bp fragments, respectively, for the wild-type and mutant alleles. The set of 3 primers for the long arm were LAN-F or LAW-F and LAC-R, yielding 429-bp and 222-bp fragments for the wild-type allele and mutant alleles, respectively (Supplemental Figure 1).

Mice were housed in autoclaved cages under specific pathogen–free conditions, fed commercially prepared pellet diet, given UV-irradiated water ad libitum, and maintained on a 12-hour-light/12-hour-dark cycle.

Histopathology of mouse samples. To label S-phase cells in wild-type and mutant mice, BrdU (50 mg/kg body weight) was injected into the peritoneal cavity as described previously, with a modification (32). One hour after injection, mice were killed by cervical dislocation. Along with duodenums, stomachs were removed, opened along the greater curvature, flattened by pinning, and fixed in 20% buffered formalin for 48 hours. Each stomach was cut longitudinally into 5 pieces of equal width and embedded in paraffin. Serial 3-μm sections were prepared and stained with H&E and Alcian blue (pH 2.5)/PAS (AB-PAS). In addition, tissues, such as the jejunum, proximal and distal colons, pancreas, liver, kidney, lung, heart, and spleen, were removed, and sections for H&E staining were similarly prepared. Gastric mucosal thickness was analyzed based on images of AB-PAS–stained sections. Briefly, a well-oriented representative pyloric gland was selected for each mouse, and mucosal thickness was measured. Muco-

sal thickness of the fundic mucosa was also measured in a similar way. Histopathology of mouse gastric mucosa was done basically according to WHO classification criteria for human gastric cancer (30). Inflammation scores in the gastric antrum were determined according to criteria of Nolan et al. (33). Briefly, inflammatory cell infiltration of the gastric mucosa by mononuclear cells and neutrophils was scored as follows: 1, mild multifocal; 2, mild widespread or moderate multifocal; 3, mild widespread and moderate multifocal or severe multifocal; 4, moderate widespread; 5, moderate widespread and severe multifocal; and 6, severe widespread.

Immunohistochemistry. Expression of αGlcNAc and MUC6 in human samples, and αGlcNAc, MUC2, BrdU, cleaved caspase-3, CD31, and the pan-macrophage marker F4/80 in mouse samples, was analyzed by immunohistochemistry. Deparaffinized tissue specimens were subjected to immunohistochemistry using primary antibodies, including anti-αGlcNAc (HIK1083) (Kanto Chemical Co. Inc.), anti-human MUC6 (CLH5) (Novo-Castra), anti-MUC2 (H-300) (Santa Cruz Biotechnology Inc.), anti-BrdU (Bu20a) (DakoCytomation), anti-cleaved caspase-3 (Asp175) (Cell Signaling Technology), anti-CD31 (SZ31) (Dianova), and anti-F4/80 (CI:A3-1) (Novus Biologicals). Before immunostaining, antigen retrieval was carried out by microwaving tissue sections in 10 mM citrate buffer (pH 6.0) for 30 minutes for anti-MUC2 and anti-cleaved caspase-3 antibodies or in 10 mM Tris-HCl buffer (pH 8.0) containing 1 mM EDTA for 30 minutes for anti-MUC6 and anti-CD31 antibodies. For anti-F4/80 antibody, tissue sections were digested with 0.25% trypsin 250 (Difco) at 37°C for 30 minutes. For anti-BrdU antibody, tissue sections were treated with 4 N HCl for 30 minutes and then digested with 0.25% trypsin 250 at 37°C for 30 minutes. Secondary antibody used for human samples was anti-mouse immunoglobulin conjugated with HRP. Immunodetection of mouse samples was carried out using a Histofine Mousestain Kit (Nichirei Biosciences) for anti-αGlcNAc and anti-CD31 antibodies, anti-rabbit immunoglobulin antibody conjugated with HRP for anti-MUC2 and anti-cleaved caspase-3 antibodies, or anti-rat immunoglobulin antibody conjugated with HRP for anti-F4/80 antibody. Peroxidase activity was visualized with diaminobenzidine-H_2O_2 solution. A control experiment was done omitting the primary antibody, and no specific staining was seen.

The BrdU-positive labeling index in mouse gastric mucosa was determined by comparing the number of BrdU-positive epithelial cells to the total number of epithelial cells contained in a rectangular sample of 100-μm breadth covering the entire gastric mucosa, and the mean value of triplicate measurements at different areas was obtained in each mouse. The number of CD31-positive and F4/80-positive cells was determined in a defined 15,000 μm^2 area, with the highest positive cell density in the pyloric mucosa, and the mean value of triplicate measurements in different areas was calculated. Because cleaved caspase-3–positive cells were rarely seen in the gastric mucosa, the number of positive cells was determined by scanning the entire pyloric mucosa area in each mouse and determining cell number per 1 mm^2 unit area.

Oligosaccharide analysis of gastric O-glycans. Mouse gastric mucins were extracted from glandular stomachs of 10-week-old *A4gnt*$^{+/+}$ and *A4gnt*$^{-/-}$ mice (2 mice each) and purified as described previously (34). Briefly, the mucosa (~80 mg each) was scraped off with a glass slide and gently homogenized by hand using a glass homogenizer cooled to 0°C in ice-cold 6 M guanidine hydrochloride (GuHCl) (pH 7.4), containing 2% (v/v) Triton X-100, 50 mM Tris, 10 mM EDTA, 0.1 M dithiothreitol, 2 mM benzamidine hydrochloride, 1 mM PMSF, and 0.15 mM pepstatin A. Homogenates were stirred for 15 hours at 4°C and centrifuged at 8,000 *g* for 60 minutes.

The supernatants were alkylated with iodoacetamide and loaded onto a Sepharose CL-6B column (1.6 × 30 cm) using 4 M GuHCl (pH 7.4), containing 0.5% Triton X-100, 50 mM Tris, 10 mM EDTA, 2 mM benzamidine hydrochloride, and 1 mM PMSF as an eluent. Fractions were assayed for PAS-stained materials as described previously (35). Fractions eluting near the void volume were pooled and subjected to cesium trifluoroacetate (CsTFA) equilibrium centrifugation at 152,000 *g* for 120 hours at 10°C, with a starting density of 1.40 g/ml in CsTFA/0.4 M GuHCl. Collected fractions were assayed for PAS-stained and HIK1083 antibody-reactive materials. Mucin fractions were pooled and desalted by ethanol precipitation (34). Alkaline-borohydride treatment of mouse gastric mucins was performed according to the method of Zinn et al. (36), using 0.05 M NaOH containing 1 M $NaBH_4$ at 45°C for 15 hours. After acidification and borate removal, oligosaccharides were purified using a Bond-Elute C18 column (Varian Technologies Japan Ltd.). Oligosaccharides were then permethylated using the methods of Ciucanu and Costell (37). For MALDI-TOF–mass spectrometry (MALDI-TOF-MS) analysis of oligosaccharides, spectra were acquired on an autoflex III mass spectrometer (Bruker Daltonics) equipped with a LIFT-MS/MS facility. 2,5-Dihydro benzoic acid served as the matrix, positive ion mode was used, and all spectra were measured in reflectron mode. A portion of the matrix solution (1 μl) was applied to a stainless steel target, to which a solution (1 μl) of oligosaccharides was added. The target was dried at ambient temperature for several minutes. Lacto-*N*-fucopentaose I, angiotensin, and ACTH 1-24 peptide were used for the mass calibration. Glycan A (GlcNAcα1-4Galβ1-4GlcNAcβ1-6[GlcNAcα1-4Galβ1-3]GalNAc-ol) and Glycan B (Fucα1-2Galβ1-4GlcNAcβ1-6[GlcNAcα1-4Galβ1-3]GalNAc-ol), purchased from Kanto Chemical Co. Inc., served as positive controls. Fragment ion analysis by tandem mass spectrometry after laser-induced dissociation was performed according to the manufacturer's operation manual.

DNA microarray analysis. Total RNA was isolated from gastric mucosa stripped from the muscular layer of the glandular stomachs of *A4gnt*$^{-/-}$ and *A4gnt*$^{+/+}$ mice at 5, 10, and 50 weeks of age using an RNeasy Kit (Qiagen). One mouse per genotype and age was examined, since gastric mucosa of *A4gnt*$^{-/-}$ mice showed consistent histopathology in each group examined — namely, hyperplasia at 5 weeks of age, low-grade dysplasia at 10 weeks, and adenocarcinoma at 50 weeks (see Supplemental Figure 3). RNA quality was assessed using an Agilent 2100 BioAnalyzer, and Cy3-labeled cRNA was synthesized using a Quick Amp Labeling Kit (Agilent Technologies), according to the manufacture's protocol. 1.65 μg Cy3-labeled cRNA were heat fragmented and applied to Agilent Whole Murine Genome Oligo ver. 2 (4 × 44 K) arrays using a Gene Expression Hybridization Kit (Agilent Technologies), and hybridization was carried out at 65°C for 17 hours. Washing was performed using a Gene Expression Wash Pack (Agilent Technologies). Slides were scanned using an Agilent Technologies Microarray Scanner, and images were processed by Feature Extraction software (Agilent Technologies) with background correction. After normalization and data filtering of the raw date output files, log-fold changes in gene expression in *A4gnt*$^{-/-}$ mice compared with those in *A4gnt*$^{+/+}$ mice at each age were analyzed to determine consistently upregulated and downregulated genes, using a 2-fold change as the cut-off using GeneSpring GX 11.0 software (Agilent Technologies). Upregulated and downregulated genes were further clustered into functional gene groups using ontology analysis with GeneSpring GX 11.0 software. Microarray data are available on the MIAME-compliant GEO database (accession number GSE31074; http://www.ncbi.nlm.nih.gov/geo/query/acc.cgi?acc=GSE31074).

Quantitative RT-PCR. RNA samples were prepared from formalin-fixed, paraffin-embedded tissue blocks from glandular stomachs (n = 5 for 5-week-old *A4gnt*$^{+/+}$ mice; n = 6 for other groups). To avoid contamination of the forestomach and duodenum adjacent to the glandular stomach, the borders between these areas were marked as described previously on H&E-stained tissue slides (38). By referring to the marked areas on

H&E-stained tissue slides, shallow incisions were made into the relevant tissue blocks along borders using a razor blade. Then, 3 slices of 10-μm thickness were prepared and transferred to a sterile 1.5 ml tube for total RNA extraction using an RNeasy FFPE Kit plus deparaffinization solution (Qiagen), according to the manufacturer's protocol. Thirteen μl of a solution containing 3 μg of RNA isolated from the glandular stomach of mice, 0.5 μl of 0.5 mg/ml random primers (Promega), 0.5 μl of 0.5 mg/ml oligo-dT primers (Promega), and 1 μl of a 2.5 mM dNTP mixture was denatured at 65°C for 5 minutes and then placed on ice. For single-stranded cDNA synthesis, samples were incubated with 1 μl of 200 U/ml SuperScript III (Invitrogen), 1 μl of 0.1 M dithiothreitol, 1 μl of 40 U/ml RNasin Plus RNase inhibitor (Promega), and 4 μl of 5× Fast Strand buffer (Invitrogen) at 50°C for 1 hour. Heating at 70°C for 10 minutes terminated the reaction.

Quantitative RT-PCR analysis was achieved using the 7300 Real-Time PCR System (Applied Biosystems). Premixed reagents containing primers and TaqMan probes for selected genes, including *Grem1* (Assay ID Mm00488615_s1), *Cxcl1* (Mm00433859_m1), *Ccl2* (Mm00441242_m1), *Cxcl5* (Mm00436451_g1), *Il11* (Mm00434162_m1), *Hgf* (Mm01135193_m1), *Il1b* (Mm01336189_m1), *Fgf7* (Mm00433291_m1), *Amh* (Mm00431795_g1), *Egf* (Mm00438696_m1), and *Pthlh* (Mm00436057_m1), plus *Gapdh* (Mm99999915_g1) for normalization, were purchased from Applied Biosystems. Using 96-well optical plates, a 20 μl solution containing 10 μl of 2x TaqMan Universal Master Mix (Applied Biosystems), 9 μl of cDNA sample, and 1 μl of 20× premixed reagents containing primers and TaqMan probe were added to each well. Plates were heated to 50°C for 2 minutes and 95°C for 10 minutes and then subjected to 50 thermal cycles (95°C, 15 seconds; 60°C, 1 minute). Specific mRNA expression was normalized to *Gapdh*, and the comparative CT value was determined by defining the median value of mRNA expression in 5-week-old $A4gnt^{+/+}$ mice as 1.0. The data were reported as mean ± SEM (n = 5 for 5-week-old $A4gnt^{+/+}$ mice; n = 6 for other groups).

Administration of celecoxib. $A4gnt^{-/-}$ mice (n = 4) were orally administered the selective Cox-2 inhibitor celecoxib (BioVision Inc.) (200 mg/kg/d in water) from 6 to 10 weeks of age. Control $A4gnt^{-/-}$ mice (n = 3) received the same volume of water without drug. Mice were sacrificed by cervical dislocation, and histopathology of gastric mucosa was examined by H&E staining.

Statistics. Statistical analysis was carried out using Ekuseru-Toukei 2006 software (Social Survey Research Information Co. Ltd.). Significance was evaluated by the 2-tailed Wilcoxon matched-pair test (for human samples) and unpaired 2-tailed Student's t test (for mouse samples). All statistical data are presented as mean ± SEM, and a P value of less than 0.05 was considered significant.

Study approval. The collection and use of all human pathology specimens for research presented here were approved by the Ethical Committee of Shinshu University School of Medicine (Matsumoto, Japan). Because the diagnostic use of these samples was completed before the study, no risk to the involved patients was predicted. In addition, these samples were coded to protect patient anonymity. Thus, no informed consent was required. The protocol for animal experiments was approved by the Animal Care Committee of Shinshu University (Matsumoto, Japan) and conducted in accordance with guidelines for the use of laboratory animals at Shinshu University.

Acknowledgments

This work was supported by Grants-in-Aid for Scientific Research 21390104 from the Japan Society for the Promotion of Science and Priority Area 1408221 from the Ministry of Education, Culture, Sports, Science and Technology of Japan (to J. Nakayama) and NIH grant P01 CA071932 (to M. Fukuda). We thank S. Taki, M. Takamoto, Y. Ito, and members of our laboratories for discussion; E. Ruoslahti and E. Lamar for critical reading of the manuscript; and K. Watanabe, H. Matsuura, T. Nishizawa, M. Watanabe, and S. Fujii for technical assistance.

Received for publication May 19, 2011, and accepted in revised form December 21, 2011.

Address correspondence to: Jun Nakayama, Department of Molecular Pathology, Shinshu University Graduate School of Medicine, Matsumoto, Japan. Phone: 81.263.37.3394; Fax: 81.263.37.2581; E-mail: jnaka@shinshu-u.ac.jp.

Shuichi Yokosawa's present address is: Department of Medicine, Shinshu University School of Medicine, Matsumoto, Japan.

Takashi Muraki's present address is: Department of Medicine, Shinshu University School of Medicine, Matsumoto, Japan.

1. Ota H, Katsuyama T, Ishii K, Nakayama J, Shiozawa T, Tsukahara Y. A dual staining method for identifying mucins of different gastric epithelial mucous cells. *Histochem J*. 1991;23(1):22–28.
2. Ishihara K, et al. Peripheral α-linked N-acetylglucosamine on the carbohydrate moiety of mucin derived from mammalian gastric gland mucous cells: epitope recognized by a newly characterized monoclonal antibody. *Biochem J*. 1996;318(pt 2):409–416.
3. Zhang MX, et al. Immunohistochemical demonstration of α1,4-N-acetylglucosaminyltransferase that forms GlcNAcα1,4Galβ residues in human gastrointestinal mucosa. *J Histochem Cytochem*. 2001; 49(5):587–596.
4. Nakamura N, et al. Histochemical reactivity of normal, metaplastic, and neoplastic tissues to α-linked N-acetylglucosamine residue-specific monoclonal antibody HIK1083. *J Histochem Cytochem*. 1998;46(7):793–801.
5. Nakayama J, Yeh JC, Misra AK, Ito S, Katsuyama T, Fukuda M. Expression cloning of a human α1,4-N-acetylglucosaminyltransferase that forms GlcNAcα1→4Galβ→R, a glycan specifically expressed in the gastric gland mucous cell-type mucin. *Proc Natl Acad Sci U S A*. 1999;96(16):8991–8996.
6. Peek RM Jr, Blaser MJ. Helicobacter pylori and gastrointestinal tract adenocarcinomas. *Nat Rev Cancer*. 2002;2(1):28–37.
7. Kawakubo M, et al. Natural antibiotic function of a human gastric mucin against Helicobacter pylori infection. *Science*. 2004;305(5686):1003–1006.
8. Hidaka E, et al. Helicobacter pylori and two ultrastructurally distinct layers of gastric mucous cell mucins in the surface mucous gel layer. *Gut*. 2001; 49(4):474–480.
9. Reis CA, et al. Intestinal metaplasia of human stomach displays distinct patterns of mucin (MUC1, MUC2, MUC5AC, and MUC6) expression. *Cancer Res*. 1999;59(5):1003–1007.
10. Oshima H, Oshima M, Inaba K, Taketo MM. Hyperplastic gastric tumors induced by activated macrophages in COX-2/mPGES-1 transgenic mice. *EMBO J*. 2004;23(7):1669–1678.
11. Correa P. Human gastric carcinogenesis: a multistep and multifactorial process. *Cancer Res*. 1992; 52(24):6735–6740.
12. Tatematsu M, Tsukamoto T, Inada K. Stem cells and gastric cancer: role of gastric and intestinal mixed intestinal metaplasia. *Cancer Sci*. 2003; 94(2):135–141.
13. Nakajima K, et al. Expression of gastric gland mucous cell-type mucin in normal and neoplastic human tissues. *J Histochem Cytochem*. 2003; 51(12):1689–1698.
14. Mantovani A, Savino B, Locati M, Zammataro L, Allavena P, Bonecchi R. The chemokine system in cancer biology and therapy. *Cytokine Growth Factor Rev*. 2010;21(1):27–39.
15. Mantovani A, Allavena P, Sica A, Balkwill F. Cancer-related inflammation. *Nature*. 2008; 454(7203):436–444.
16. Grivennikov SI, Greten FR, Karin M. Immunity, inflammation, and cancer. *Cell*. 2010;140(6):883–899.
17. Salcedo R, et al. Human endothelial cells express CCR2 and respond to MCP-1: direct role of MCP-1 in angiogenesis and tumor progression. *Blood*. 2000; 96(1):34–40.
18. Ohta M, et al. Monocyte chemoattractant protein-1 expression correlates with macrophage infiltration and tumor vascularity in human gastric carcinomas. *Int J Oncol*. 2003;22(4):773–778.
19. Nakayama T, et al. Expression of interleukin-11 (IL-11) and IL-11 receptor α in human gastric carcinoma and IL-11 upregulates the invasive activity of human gastric carcinoma cells. *Int J Oncol*. 2007; 30(4):825–833.
20. Howlett M, et al. The interleukin-6 family cytokine interleukin-11 regulates homeostatic epithelial cell

turnover and promotes gastric tumor development. *Gastroenterology*. 2009;136(3):967–977.
21. Kosinski C, et al. Gene expression patterns of human colon tops and basal crypts and BMP antagonists as intestinal stem cell niche factors. *Proc Natl Acad Sci U S A*. 2007;104(39):15418–15423.
22. Takahashi M, et al. Hepatocyte growth factor is the most potent endogenous stimulant of rabbit gastric epithelial cell proliferation and migration in primary culture. *J Clin Invest*. 1995;95(5):1994–2003.
23. Nakazawa K, Yashiro M, Hirakawa K. Keratinocyte growth factor produced by gastric fibroblasts specifically stimulates proliferation of cancer cells from scirrhous gastric carcinoma. *Cancer Res*. 2003; 63(24):8848–8852.
24. Palmieri C, et al. Fibroblast growth factor 7, secreted by breast fibroblasts, is an interleukin-1β-induced paracrine growth factor for human breast cells. *J Endocrinol*. 2003;177(1):65–81.
25. Tu S, et al. Overexpression of interleukin-1β induces gastric inflammation and cancer and mobilizes myeloid-derived suppressor cells in mice. *Cancer Cell*. 2008;14(5):408–419.
26. Kai H, et al. Involvement of proinflammatory cytokines IL-1β and IL-6 in progression of human gastric carcinoma. *Anticancer Res*. 2005;25(2A):709–713.
27. Barbie TU, Barbie DA, MacLaughlin DT, Maheswaran S, Donahoe PK. Mullerian inhibiting substance inhibits cervical cancer cell growth via a pathway involving p130 and p107. *Proc Natl Acad Sci U S A*. 2003;100(26):15601–15606.
28. Sipponen P, Hyvärinen H. Role of Helicobacter pylori in the pathogenesis of gastritis, peptic ulcer and gastric cancer. *Scand J Gastroenterol Suppl*. 1993;196:3–6.
29. Ohtsubo K, Marth JD. Glycosylation in cellular mechanisms of health and disease. *Cell*. 2006; 126(5):855–867.
30. Fenoglio-Preiser C, et al. Gastric carcinoma. In: Hamilton SR, Aaltonen LA, eds. *Pathology and Genetics of Tumours of the Digestive System*. Lyon, France: IARC Press; 2000:39–52.
31. Muyrers JP, Zhang Y, Benes V, Testa G, Ansorge W, Stewart AF. Point mutation of bacterial artificial chromosomes by ET recombination. *EMBO Rep*. 2000; 1(3):239–243.
32. Maeyama H, Furuwatari C, Ota H, Akamatsu T, Nakayama J, Katsuyama T. Histone H3 messenger RNA in situ hybridization for identifying proliferating cells in formalin–fixed rat gastric mucosa. *Histochem J*. 1997;29(11–12):867–873.
33. Nolan KJ, et al. In vivo behavior of a Helicobacter pylori SS1 nixA mutant with reduced urease activity. *Infect Immun*. 2002;70(2):685–691.
34. Goso Y, Ishihara K, Kurihara M, Sugaya T, Hotta K. Rat gastric mucins recognized by monoclonal antibodies RGM21 and HIK1083: isolation of mucin species characteristic of the surface and glandular mucosa. *J Biochem*. 1999;126(2):375–381.
35. Goso Y, Hotta K. Dot blot analysis of rat gastric mucin using histochemical staining methods. *Anal Biochem*. 1994;223(2):274–279.
36. Zinn AB, Plantner JJ, Carlson DM. Nature of linkages between protein core and oligosaccharides. In: Horowitz MI, Pigman W, eds. *The Glycoconjugates*. Vol. 1. New York, New York, USA: Academic Press; 1977:69–85.
37. Ciucanu I, Costello CE. Elimination of oxidative degradation during the per-O-methylation of carbohydrates. *J Am Chem Soc*. 2003;125(52):16213–16219.
38. Ito Y, et al. The utility of formalin-fixed and paraffin-embedded tissue blocks for quantitative analysis of N-acetylgalactosamine 4-sulfate 6-O-sulfotransferase mRNA expressed by colorectal cancer cells. *Acta Histochem Cytochem*. 2007;40(2):53–59.